# Stimulated Raman Scattering Microscopy with a Robust Fibre Laser Source

# Stimulated Raman Scattering (SRS) Microscopy with a Robust Fiber Laser Source

Christian W. Freudiger[1,2,†], Wenlong Yang[2,†], Gary R. Holtom[2], Nasser Peyghambarian[3], X. Sunney Xie[2*], Khanh Q. Kieu[3,*]

[1] INVENIO IMAGING, Inc., Cambridge, Massachusetts 02142 (USA)

[2] Department of Chemistry and Chemical Biology, Harvard University, Cambridge, Massachusetts 02138 (USA)

[3] College of Optical Science, University of Arizona, Tucson, Arizona 85721 (USA)

[†]Authors have contributed equally to this work.

*email: X. Sunney Xie [xie@chemistry.harvard.edu] or Khanh Kieu [kkieu@optics.arizona.edu]

**Abstract:** Stimulated Raman Scattering (SRS) microscopy allows label-free chemical imaging and has enabled exciting applications in biology, material science, and medicine. It provides a major advantage in imaging speed over spontaneous Raman scattering and has improved image contrast and spectral fidelity compared to coherent anti-Stokes Raman (CARS). Wider adoption of the technique has, however, been hindered by the need for a costly and environmentally sensitive tunable ultra-fast dual-wavelength source. We present the development of an optimized all-fiber laser system based on the optical synchronization of two picosecond power amplifiers. To circumvent the high-frequency laser noise intrinsic to amplified fiber laser, we have further developed a high-speed noise cancellation system based on voltage-subtraction auto-balanced detection. We demonstrate uncompromised imaging performance of our fiber-laser based SRS microscope with shot-noise limited sensitivity and an imaging speed up to 1 frame/s.

In coherent Raman scattering (CRS) microscopy[1-6], the sample is illuminated with two synchronized laser beams, which are commonly referred to as pump and Stokes. If their frequency difference matches a molecular vibrational frequency of the sample, the targeted population is excited from the ground to the vibrational state (Fig. 1a)[7]. In contrast to spontaneous Raman scattering, the stimulated transition from the virtual to the vibrational state by the presence of the Stokes field results in an amplification of the molecular transition rate and allows label-free chemical imaging at speeds up to video-rate[8,9].

Various detection schemes have been developed to probe this amplified Raman signal in microscopy. The easier to implement coherent anti-Stokes Raman scattering (CARS)[1,2] suffers from a nonresonant background signal that limits sensitivity for dilute species[10,11]. Stimulated Raman scattering (SRS) is free from this background and its excitation spectra match well-documented spontaneous Raman spectra[3-6]. The typical implementation of SRS[12] detects the small intensity loss of the transmitted pump beam with a high-frequency modulation transfer scheme that takes advantage of the fact that laser noise of solid-state lasers commonly reduces to shot-noise at high frequencies[13].

SRS has been applied extensively in bio-medical research[14] and achieving high sensitivity under biocompatible excitations conditions is a key challenge. As a nonlinear optical process, SRS benefits from pulsed near-IR lasers, which generate high signal levels at moderate average power. Best signal levels are obtained by narrowband excitation of a single vibrational frequency. Species with spectrally mixed bands can be distinguished by multi-spectral imaging, where the frequency difference of the pump and Stokes beams is tuned between image frames[15,16] or lines[17]. An ideal light source for SRS provides two tightly synchronized and quickly tunable pulse trains with bandwidths narrower than a typical Raman linewidth ($<20 cm^{-1}$).

The current gold-standard laser system for SRS is a synchronously pumped picosecond optical parametric oscillator (OPO)[18], which has vanishing timing jitter compared to electronically

synchronized lasers[19]. Its cost is high and the free-space cavity is sensitive to environmental changes. Fiber laser technology has the potential to overcome these limitations as components are inexpensive and light-guiding by the fiber core avoids misalignment. Different concepts have been proposed[20-26]. From the free-space OPO system, we have learned that optical synchronization avoids timing jitter and improves long-term stability. However, previous approaches to fiber-based optically synchronized systems are less than optimal: super-continuum generation (SC)[20-22] does not scale to sufficiently high power, implementation of a fiber-based OPO has proven difficult[24], and un-seeded four-wave mixing requires low-repetition rates[23], which ultimately limit the imaging speed. Here we combine the advantages of optical synchronization with straight-forward power scaling in fiber amplifiers.

A remaining challenge of amplified fiber lasers compared to high-power free-space lasers is the presence of high-frequency laser noise[22,26]. We present the implementation of a noise suppression scheme based on auto-balanced detection[27,28]. Compared to previous implementations that suffer from low speed[21] or a limited noise cancellation bandwidth[26], we have developed detection electronics optimized for high-speed microscopy. We present sensitive SRS imaging with uncompromised performance with our novel fiber laser source.

**Results.** The laser system is based on the key realization that the difference frequency of the two major fiber gain media, Erbium (Er) and Ytterbium (Yb), corresponds to the high-wavenumber region of Raman spectra[25], where most SRS imaging is performed. We have implemented an all-fiber dual-wavelength laser system based on optical synchronization of two picosecond amplifiers using a broadband SC and have optimized the pulse parameters for high-speed SRS imaging.

Fig. 1b shows a detailed schematic of our tunable dual-wavelength fiber laser source. It starts with an Er-doped fiber oscillator at 1560nm that is mode-locked with a carbon nanotube (CNT) saturable absorber[29] at a repetition rate of 59MHz. The output power of the oscillator is 7mW and is split into two arms to generate the pump and Stokes beams for SRS.

The first arm is amplified to 80mW in a normal dispersion Er-doped pre-amplifier. Its output is broadened due to self-phase modulation (SPM) and we use a narrowband filter to reduce the bandwidth for SRS. The power (about 2.2mW after filtering) is restored in a low-nonlinearity Er-doped power amplifier. Its output could directly provide the Stokes beam for SRS. However, most multi-photon microscopes are optimized for transmission in the wavelength range from 400-1100nm and we frequency double the output in a periodically poled lithium niobate (PPLN) crystal (Covesion, MSHG1550-1.0-10). With a conversion efficiency of ~45%, we obtain a near-IR pump beam for SRS with up to 75mW average power.

The second arm is frequency shifted in an SC unit based on a highly nonlinear fiber (HNLF). Stable SC generation requires the use of a short piece of HNLF. By careful optimization of the splice between the SMF and HNLF, it is possible to reduce the spice loss to <1dB, enabling an all-fiber implementation. The output covers a range from 950nm to >1700nm (detection limit of the optical spectrum analyzer)[30]. We then use an Yb-doped pre-amplifier to increase the power of the spectral range around 1 micron to 40mW[30,31] and a narrowband filter to produce a picosecond pulse train that can be amplified in a low-nonlinearity Yb-doped power amplifier. We now have a narrowband Stokes beam with up to 120mW average power that is synchronized to the oscillator, and thus the pump beam.

Precise tuning of the difference frequency between pump and Stokes beams is achieved with motorized tunable filters. The outputs of the Er- and Yb-doped amplifiers are tunable from 1530nm to 1590nm (Fig. 2a) and from 1010nm to 1060nm (Fig. 2b), respectively. For fast tuning, we keep the pump beam fixed (the phase-matching wavelength of the PPLN crystal is temperature controlled) and only tune the Stokes beam. Specifically, to access Raman spectra in the high-wavenumber region from 2800 to 3100 $cm^{-1}$, we frequency double the fixed wavelength Er-arm at 1580nm to 790 nm (Fig. 2c) and tune the Yb-arm from 1015nm to 1045nm with <0.1nm tuning accuracy (Agiltron, FOTF-01-6).

We optimized the pulse parameters specifically for SRS imaging of biological specimens by choosing the bandwidths of the narrowband filters and the length of the oscillator cavity. Our theoretical

modeling (see supplementary materials) indicates that the SNR does not depend on the exact laser duty factor (Sup. Fig. S1a) as nonlinear photo-damage limits the maximum permissible peak power[32-34]. However, at lower duty factors, higher average power is required to achieve the same SNR (Sup. Fig. 1b). With the ANSI safety standard for clinical use of 30 mW at 800 nm in mind (see supplementary materials), it is thus advantageous to increase the duty factor compared to the solid-state OPO laser system which has a 6ps pulse duration and 80MHz repetition rate.

We chose filters with a bandwidth of 1.2nm (Fig. 2b), which approaches the required spectral resolution limit for SRS. Figure 2d shows the autocorrelation of the Stokes beam at 1030 nm. The pulse duration of 1.0ps was calculated by dividing the full width at half maximum (FWHM) by the square-root of two. This corresponds to a time-bandwidth product of a transform limited pulse and, at 59 MHz repetition rate, provides a duty factor increase of about 8x compared to the solid-state OPO laser system. Figure 2e shows the autocorrelation of the pump beam with a pulse duration of 4.0ps. The time-bandwidth product of 0.68 is about 2x larger than the transform limit, which is due to the natural bandwidth reduction during frequency doubling and a slight chirp, which arises from the choice of a too long PPLN crystal. In a further optimized version of the laser source, we will aim to match the pulse duration of pump and Stokes pulses.

The two beams are spatially overlapped with a free-space dichroic mirror. The rough time delay is adjusted by adding un-doped fiber before the Yb-doped power amplifier. Fine delay is obtained by adjusting a mechanical delay line (Fig. 1b) while monitoring the sum-frequency generation (SFG) signal from a BBO crystal. This setup was also used to measure the cross-correlation of the two pulse trains and determine the timing jitter. Figure 2f shows a 5 minutes time-trace of the SFG signal at the half-maximum of the cross-correlation. Using the slope of the cross-correlation to convert from amplitude to timing fluctuations, the timing jitter is estimated to be <24fs. Such an approach only provides an upper limit estimate as laser intensity fluctuations can be falsely interpreted as timing jitter.

However, it is sufficient to demonstrate that the timing jitter is much smaller than the cross-correlation bandwidth of 4.4ps and does not affect the SRS imaging capabilities.

After careful optimization of the noise performance of the Er-arm, we obtained a pump beam that is about 27dB above the shot-noise floor at 28mW average power (Fig. S3). Anything other than shot-noise limited performance is not acceptable for SRS microscopy, as it limits the ability to detect low-concentration molecular species. The general idea of balanced detection (Fig. 3a) is that a portion of the pump beam can be sampled at the laser output (Fig. 1b). Laser noise other than the shot-noise is common to both the sample and reference arm and subtracting the two results in suppression of such common mode noise. As the modulated signal only appears in the sample arm, it is not subtracted and can be detected with demodulation electronics (e.g. lock-in amplifier) with shot-noise limited sensitivity (Fig. 3a).

In theory, balanced detection can reduce the laser noise to 3dB above the shot-noise because it also introduces the shot-noise of the reference arm. In practice, noise cancellation depends on the exact balance of the two arms. For example, if the intensity of the sample arm is only 90% of the reference arm, noise is suppressed by a factor of 10 or 20dB. Application of the technique to microscopy would thus be limited by varying sample transmission. To ensure maximum suppression independent of sample transmission we implement "auto"-balanced detection and rely on the DC signals from both arms to control the gain of the reference arm to balance the signals prior to subtraction. This approach takes advantage of the time-scale separation of the modulation, the auto-balancing speed, and the pixel-dwell-time. However, commercially available balanced detectors do not meet these timing requirements and their use drastically reduces the imaging speed[22].

To overcome this limitation, we have developed a voltage-subtraction auto-balanced detector for the specific requirements in high-speed microscopy. A detailed schematic is shown in Supplementary Figure S2. Identical large-area silicon diodes are used for the sample and reference arms to accommodate high optical power. The AC and DC signals of each arm are then separated. The AC

signals are filtered around 10MHz and pre-amplified by trans-impedance amplifiers to overcome electronic noise. A four-channel variable gain amplifier (VGA) amplifies the filtered AC and DC signals of the two arms and a PID feed-back circuit is used to control the gain of the reference arm to lock the DC levels. Because AC and DC signals experience the same gain in each channel, this generates the auto-balancing of the AC signals prior to subtraction in a differential amplifier.

Our auto-balanced detector allows a noise suppression of >40dB at 10MHz (Fig. 3b), which is significantly more than the laser excess noise. We thus achieve shot-noise limited detection sensitivity (Fig. 3c). The noise suppression bandwidth of our implementation is currently limited by the dispersion of the specific phase-shifters, which is not fundamental and is sufficiently large (500kHz) to allow removal of all excess noise at the sampling speeds required for 1 frame/s imaging. The 3dB point of the auto-balancing loop (data not show) is chosen at about 500kHz to compensate for pixel-to-pixel transmission variation.

For SRS imaging, the Stokes beam is modulated at 10MHz with an electro-optic modulator (Thorlabs, EO-AM-NR-C2) and combined with the pump beam using a dichroic mirror. The collinear beams are directed into a beam-scanning microscope (Olympus, IX71) and focused into the sample with a water immersion objective (Olympus, UPLANSAPO 60XW, 1.2NA). The transmitted beams are collected with an oil immersion condenser (Nikon, 1.4NA), the Stokes beam is blocked with a high-OD filter (Chroma, CARS890/220), and the pump beam is detected with the signal arm of the auto-balanced detector. The sample beam is generated with a polarization beam splitter and the rough balance is set with a half wave plate prior to imaging. The output of the auto-balanced detector is then sent to a custom lock-in amplifier[9] to detect the 10MHz SRS signal.

Figures 3d and 3e show SRS images of 1.1μm polystyrene beads acquired at an imaging speed of 1 frame/s and with 24mW power at the focus with (Fig. 3d) and without auto-balancing (Fig. 3e). Balanced detection improves SNR by 10.6x from 0.5 to 5.3. No image artifact due to varying sample transmission is visible even at the edges of the beads (Sup. Fig. S4).

Fig. 4a shows multi-color SRS imaging of mouse skin samples. The green channel in Fig. 4a was acquired at the $CH_2$-streching vibration of lipids ($2850cm^{-1}$) and the red channel at the $CH_3$-streaching vibration of proteins ($2950cm^{-1}$). The image shows a lipid-rich sebaceous gland wrapping around a protein-rich hair. Figure 4b shows a 100μm depth stack acquired every 1μm at a frame-rate of 1 frame/s (Sup. Video 1 shows the complete z-stack). This presents the fastest SRS imaging experiment performed with a fiber laser source to date and reaches the performance of the more expensive state-of-the-art solid-state laser system.

To demonstrate the "robustness" of the laser system, we performed imaging on a table that was not vibration isolated and in an environment that was not climate controlled (Sup. Fig. S5). We also demonstrated the performance of the laser to external shock (Sup. Video 2) and ultra-long-term imaging over 44 hours without adjusting the laser (Sup. Video 3).

**Discussions.** We have developed a dual-wavelength fiber laser source for SRS microscopy that is precisely tunable over the entire high-wavenumber region of Raman spectra, where most SRS imaging is performed. To reach the performance of solid-state laser systems, we optimized the laser amplifiers and developed a broad-band voltage-subtraction auto-balanced detector. We demonstrate SRS imaging at an imaging speed up to 1 frame/s with shot-noise limited sensitivity. The major advantages of our fiber laser SRS system are (1) operation that does not require vibration isolated optical table, (2) operation in environments that are not climate controlled, and (3) reduced cost. It has the promise to extend the use of SRS microscopy to non-expert users and enable clinical applications. Toward this goal, demonstrating high-quality imaging at excitation powers that are compliant with the ANSI safety standard provides a major milestone.

The major limitation of the current proof-of-concept implementation is the use of non-polarization maintaining (PM) components and adjustment of the polarization state of the output is required to maintain maximum SRS signal. All components are available as PM version and an all-PM design is conceivable based on the same recipe. The use of large-mode area (LMA) components will further

reduce SPM broadening and increase spectral fidelity. Attention will have to be paid to achieve better matching of the pulse durations of pump and Stokes beams. All-fiber delivery is further required to fully take advantage of the properties of fiber-lasers. Finally, system integration of the microscope and the fiber laser will enable automated spectral SRS imaging, and the development of an integrated hand-held SRS scanner is underway.

**Methods**

Laser spectra were measured with an optical spectrum analyzer (HP, 70951A) with a spectral resolution of 0.1nm. Optical auto-correlations were measured with a home-built background-free auto-correlator based on a 1mm BBO crystal (Witcore, BBO 6-6-1mm) and a manual delay stage. The timing jitter measurements were acquired with the same setup. Relative intensity noise (RIN) spectra were acquired with an RF spectrum analyzer (Siganlhound,USB-SA44B) following reference[35]. The bandwidth of the spectrum analyzer for the measurements of Fig. 3b,c is 400Hz. We use a large-area Si photodiode (OSI Optoelectronics, S-100CL) back-biased at 48V to provide both dynamic range as well as response time. The DC signal was separated with a bias-T (Minicircuits, ZFBT-4R2GW+) and recorded with an oscilloscope to provide the intensity calibration of the RIN measurement (Fig. S3). The shot-noise level was estimated following reference[35] given the measured DC signal. The suppression ratio of the balanced detector was measured with the RF spectrum analyzer by artificially increasing the noise of the fiber laser with an acousto-optic modulator driven by a white noise signal from an RF function generator.

**Figure Captions**

**Figure 1 | Schematic of the SRS fiber laser system. a**, Energy diagram of SRS. When the difference in photon energy between the pump and the Stokes beam matches the energy of a targeted vibrational state, $\hbar\Omega$, molecules are efficiently excited from the ground to the excited state. **b**, Schematic of the fiber laser. The Er-doped fiber oscillator is mode-locked with a carbon nanotube (CNT) saturable absorber. Its output is split into two arms to generate the pump (upper arm) and Stokes beams (lower arm). The Stokes beam is modulated at 10MHz with an electro optic modulator (EOM), temporally and spatially combined with the pump beam, and aligned into to a beam-scanning microscope. The transmitted pump beam is detected by the auto-balanced detector after the Stokes beam is blocked with an optical band pass filter. The reference beam is sampled in front of the microscope with a polarizing beam splitter (BS).

**Figure 2 | Characterization of the fiber laser source. a** & **b**, Tuning ranges of the Er- and Yb-doped fiber power amplifiers. **c**, Spectrum of frequency-doubled Er-doped amplifier output pulses with a fixed wavelength narrowband filter at 1580nm.**d** & **e**, Optical auto-correlations of the pump and Stokes (at 1030nm) pulses respectively. **f**, Measurement of the timing jitter: intensity noise at the peak (red) and half maximum (blue) of the optical cross-correlation (inset) over 5 minutes.

**Figure 3 | Auto-balanced detection. a**, Principle of balanced detection. **b** Noise suppression of the home-built auto-balanced detector optimized for 10MHz signal. **c** Noise spectrum of the fiber laser with (red) and without auto-balanced detection (blue), noise spectrum of the reference diode (green) and the theoretical shot-noise (grey). **d** & **e**, SRS image of 1.1μm polystyrene beads with (d) and without (e) auto-balanced detection. Scale bar: 5μm.

**Figure 4 | SRS spectral imaging with the fiber laser source. a**, Two color image of a sebaceous gland in mouse skin acquired at 2850cm$^{-1}$ (mainly lipids, green), 2950cm$^{-1}$ (mainly proteins, red) and the composite of the two colors. **b**,3D image stack acquired at 1 frame/s. Lines indicate the positions at which cross-sectional views were taken. Scale bar: 50μm.

# References


1 Zumbusch, A., Holtom, G.R. & Xie, X.S. Three-dimensional vibrational imaging by coherent anti-stokes raman scattering. *Phys. Rev. Lett.* **82**, 4142-4145, (1999).

2 Evans, C.L. & Xie, X.S. Coherent anti-stokes raman scattering microscopy: Chemical imaging for biology and medicine. *Annu. Rev. Anal. Chem.* **1**, 883-909, (2008).

3 Ploetz, E., Laimgruber, S., Berner, S., Zinth, W. & Gilch, P. Femtosecond stimulated raman microscopy. *Appl. Phys. B-Lasers O.* **87**, 389-393, (2007).

4 Freudiger, C.W. *et al.* Label-free biomedical imaging with high sensitivity by stimulated raman scattering microscopy. *Science* **322**, 1857-1861, (2008).

5 Ozeki, Y., Dake, F., Kajiyama, S., Fukui, K. & Itoh, K. Analysis and experimental assessment of the sensitivity of stimulated raman scattering microscopy. *Opt. Express* **17**, 3651-3658, (2009).

6 Nandakumar, P., Kovalev, A. & Volkmer, A. Vibrational imaging based on stimulated raman scattering microscopy. *New J. Phys.* **11**, 033026, (2009).

7 Bloembergen, N. The stimulated raman effect. *Am. J. Phys.* **35**, 989-1023, (1967).

8 Evans, C.L. *et al.* Chemical imaging of tissue in vivo with video-rate coherent anti-stokes raman scattering microscopy. *Proc. Natl. Acad. Sci. U. S. A.* **102**, 16807, (2005).

9 Saar, B.G. *et al.* Video-rate molecular imaging in vivo with stimulated raman scattering. *Science* **330**, 1368-1370, (2010).

10 Ganikhanov, F., Evans, C.L., Saar, B.G. & Xie, X.S. High-sensitivity vibrational imaging with frequency modulation coherent anti-stokes raman scattering (fm cars) microscopy. *Opt. Lett.* **31**, 1872-1874, (2006).

11 Min, W., Freudiger, C.W., Lu, S. & Xie, X.S. Coherent nonlinear optical imaging: Beyond fluorescence microscopy. *Annu. Rev. Phys. Chem.* **62**, 507-530, (2011).

12 Owyoung, A. Sensitivity limitations for cw stimulated raman spectroscopy. *Opt. Commun.* **22**, 323-328, (1977).

13 Ozeki, Y. *et al.* Stimulated raman scattering microscope with shot noise limited sensitivity using subharmonically synchronized laser pulses. *Opt. Express* **18**, 13708-13719, (2010).

14 Ji, M.B. *et al.* Rapid, label-free detection of brain tumors with stimulated raman scattering microscopy. *Sci. Transl. Med.* **5**, 201ra119 (2013).

15 Lin, C.Y. *et al.* Picosecond spectral coherent anti-stokes raman scattering imaging with principal component analysis of meibomian glands. *J. Biomed. Opt.* **16**, 021104-021109, (2011).

16 Ozeki, Y. *et al.* High-speed molecular spectral imaging of tissue with stimulated raman scattering. *Nat. Photonics* **6**, 845-851, (2012).

17 Kong, L.J. *et al.* Multicolor stimulated raman scattering microscopy with a rapidly tunable optical parametric oscillator. *Opt. lett.* **38**, 145-147, (2013).

18 Ganikhanov, F. *et al.* Broadly tunable dual-wavelength light source for coherent anti-stokes raman scattering microscopy. *Opt. Lett.* **31**, 1292-1294, (2006).

19 Jones, D.J. *et al.* Synchronization of two passively mode-locked, picosecond lasers within 20 fs for coherent anti-stokes raman scattering microscopy. *Rer. Sci. Instrum.* **73**, 2843-2848, (2002).

20 Pegoraro, A.F. *et al.* Optimally chirped multimodal cars microscopy based on a single ti: Sapphire oscillator. *Opt. Express* **17**, 2984-2996, (2009).

21 Krauss, G. *et al.* Compact coherent anti-stokes raman scattering microscope based on a picosecond two-color er: Fiber laser system. *Opt. Lett.* **34**, 2847-2849, (2009).
22 Gambetta, A. *et al.* Fiber-format stimulated-raman-scattering microscopy from a single laser oscillator. *Opt. Lett.* **35**, 226-228, (2010).
23 Baumgartl, M. *et al.* All-fiber laser source for cars microscopy based on fiber optical parametric frequency conversion. *Opt. Express* **20**, 4484-4493, (2012).
24 Lefrancois, S. *et al.* Fiber four-wave mixing source for coherent anti-stokes raman scattering microscopy. *Opt. Lett.* **37**, 1652-1654, (2012).
25 Bégin, S. *et al.* Coherent anti-stokes raman scattering hyperspectral tissue imaging with a wavelength-swept system. *Biomed. Opt. Express* **2**, 1296-1306, (2011).
26 Nose, K. *et al.* Sensitivity enhancement of fiber-laser-based stimulated raman scattering microscopy by collinear balanced detection technique. *Opt. Express* **20**, 13958-13965, (2012).
27 Hobbs, P.C.D. Shot noise limited optical measurements at baseband with noisy lasers. *Proc. SPIE vol. 1376, Laser Noise*, 216-221, (1990).
28 Hobbs, P.C.D. *Building electro-optical systems : Making it all work*. (Wiley, New York, 2000).
29 Kieu, K. & Mansuripur, M. Femtosecond laser pulse generation with a fiber taper embedded in carbon nanotube/polymer composite. *Opt. Lett.* **32**, 2242-2244, (2007).
30 Kieu, K., Jones, R.J. & Peyghambarian, N. High power femtosecond source near 1 micron based on an all-fiber er-doped mode-locked laser. *Opt. Express* **18**, 21350-21355, (2010).
31 Andrianov, A., Anashkina, E., Muravyev, S. & Kim, A. All-fiber design of hybrid er-doped laser/yb-doped amplifier system for high-power ultrashort pulse generation. *Opt. Lett.* **35**, 3805-3807, (2010).
32 Hopt, A. & Neher, E. Highly nonlinear photodamage in two-photon fluorescence microscopy. *Biophys. J.* **80**, 2029-2036, (2001).
33 Fu, Y., Wang, H., Shi, R. & Cheng, J.X. Characterization of photodamage in coherent anti-stokes raman scattering microscopy. *Opt. Express* **14**, 3942-3951, (2006).
34 Nan, X., Potma, E.O. & Xie, X.S. Nonperturbative chemical imaging of organelle transport in living cells with coherent anti-stokes raman scattering microscopy. *Biophys. J.* **91**, 728-735, (2006).
35 Obarski, G.E. & Hale, P.D. How to measure relative intensity noise in lasers. *Laser Focus World* **35**, 273-278, (1999).

**Acknowledgements:** We thank Philip Hobbs, James McArthur and Jay Trautman for discussions. We thank Dan Fu and Fa-Ke Lu for help with sample preparation. This material is based upon work supported by the National Science Foundation (NSF) under Grant No. 1214848 to CWF and by the Nation Institute of Health (NIH) under Grant No. 5R01EB010244 to XSX. This work was performed in part at the Center for Nanoscale Systems (CNS), a member of the National Nanotechnology Infrastructure Network (NNIN), which is supported by the NSF under Grant No. ECS-0335765. CNS is part of Harvard University.

**Materials & Correspondence:** Correspondence should be addressed to X. Sunny Xie (xie@chemistry.harvard.edu)

Address: Harvard University, 12 Oxford Street, Department of Chemistry and Chemical Biology, Cambridge, MA 02138, U. S. A.

Phone: +1-617-496-9925

Fax: +1-617-496-8709

**Author contributions:** CWF and KQK designed and characterized the fiber laser system. WY and GRH designed and characterized the auto-balanced detector. CWF and WY performed the imaging experiments. CWF, XSX, NP and KQK conceived the project and supervised its implementation. CWF, WY, KQK, NP and XSX wrote the manuscript and all authors commented on it.

**Competing financial interests:** Harvard University and University of Arizona has filed a patent application based on the current work. CWF and XSX have financial interests in INVENIO IMAGING INC. KQK has financial interests in KPhotonics LLC. Any opinions, findings, conclusions or

recommendations expressed in this material are those of the authors and do not necessarily reflect the views of the NSF or NIH.

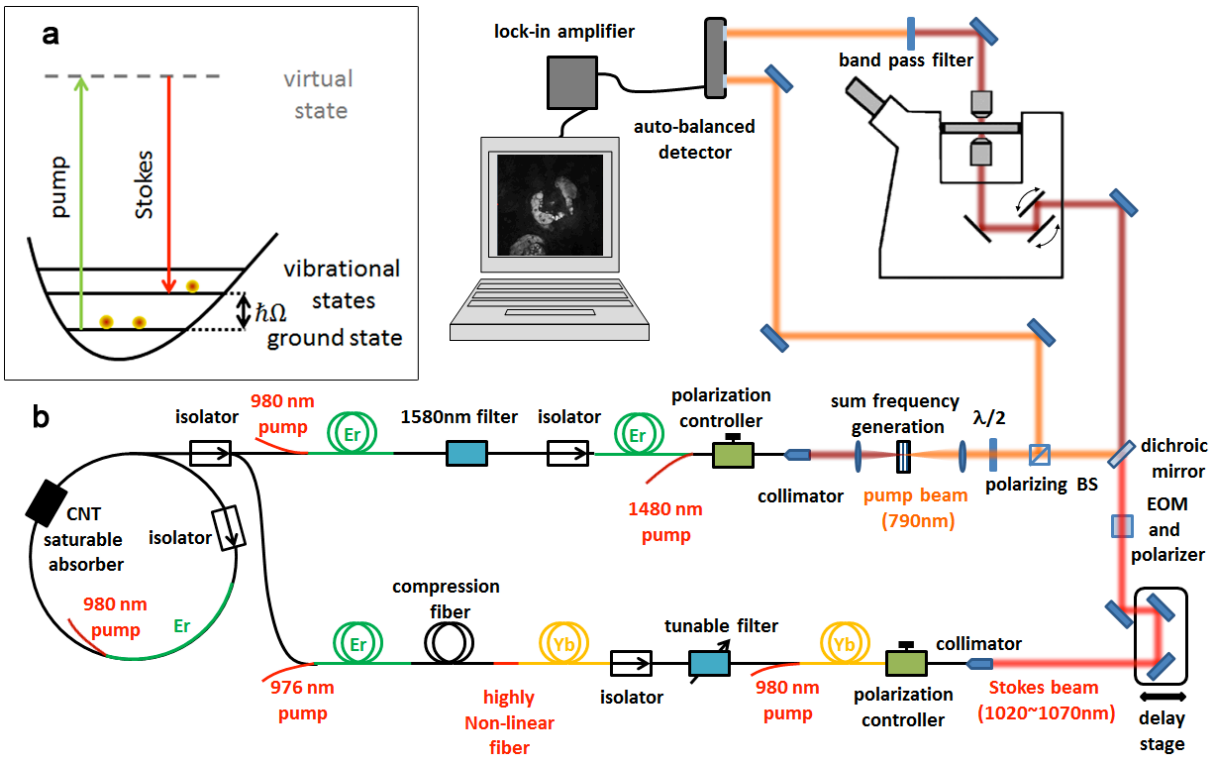


**Figure 1 | Schematic of the fiber laser system and SRS microscope. a**, Energy diagram of SRS. When the difference in photon energy between the pump and the Stokes beam matches the energy of a vibrational state of the target molecule, ħΩ, molecules are efficiently excited from the ground state to the corresponding excited state and a pump photon is absorbed (stimulated Raman loss, SRL) and a Stokes photon is generated (stimulated Raman gain, SRG). **b**, Schematic of the fiber laser. The laser system starts with an Er-doped fiber oscillator, which is mode-locked with a carbon nanotube (CNT) saturable absorber. The output is split into two arms to generate the pump (upper arm) and Stokes beams (lower arm). The Stokes beam is modulated at 10MHz with an electro optic modulator (EOM), temporally and spatially combined with the pump beam, and aligned into to a beam-scanning microscope. Transmitted beams are collected with a condenser. The pump beam is detected by the auto-balanced detector after the Stokes beam is blocked with an optical filter. The reference beam is sampled in front of the microscope with a polarizing beam splitter (BS).

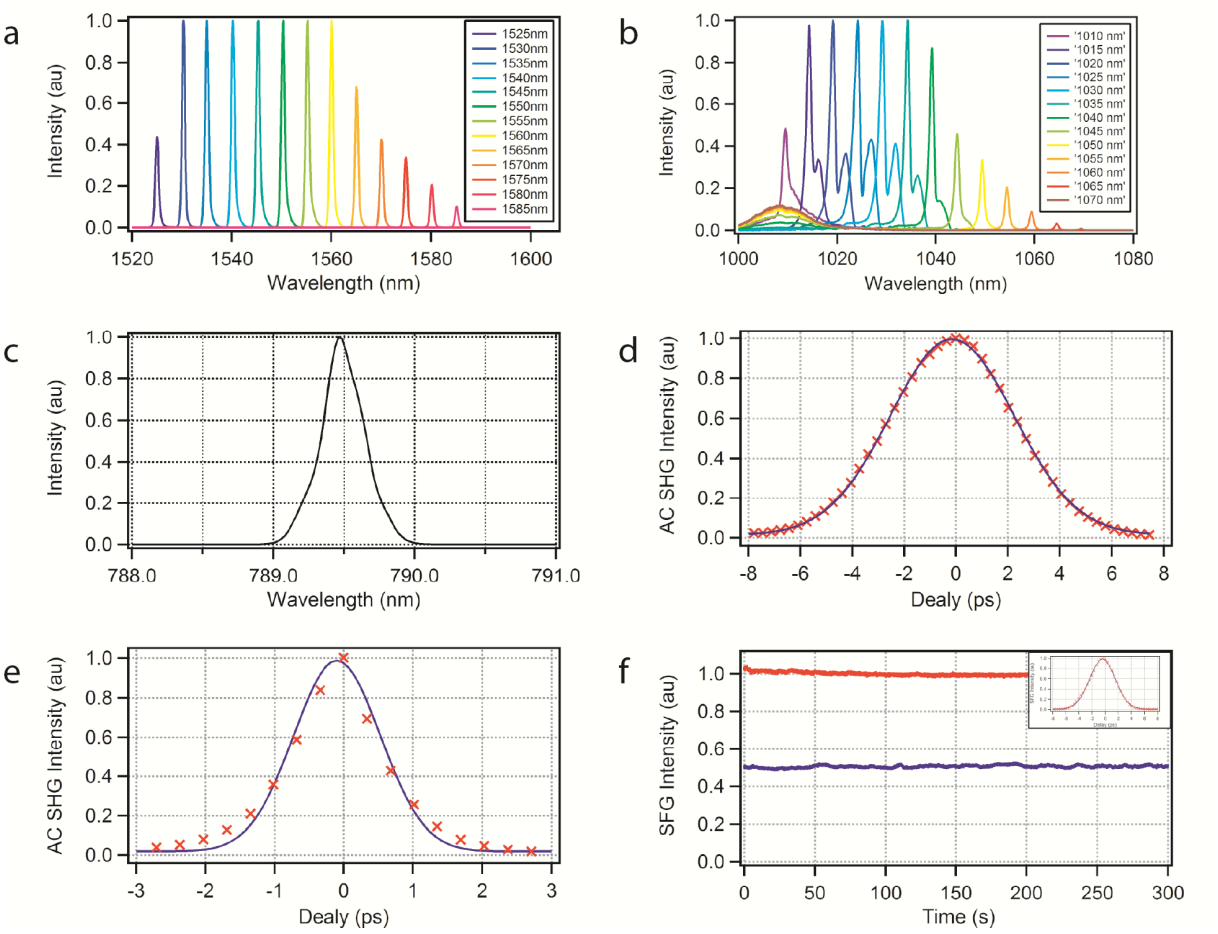


**Figure 2 | Characterization of the fiber laser source. a & b**, Tuning ranges of the Er- and Yb-doped fiber power amplifiers. The Er-arm is frequency doubled to provide the pump beam (**c**). The Yb-arm provides the Stokes beam. **d & e**, Optical auto-correlations of the pump and Stokes pulses. **f**, Measurement of the timing jitter. Intensity noise at the peak (red) and half maximum (blue) of the optical cross-correlation (inset) over 5 minutes.

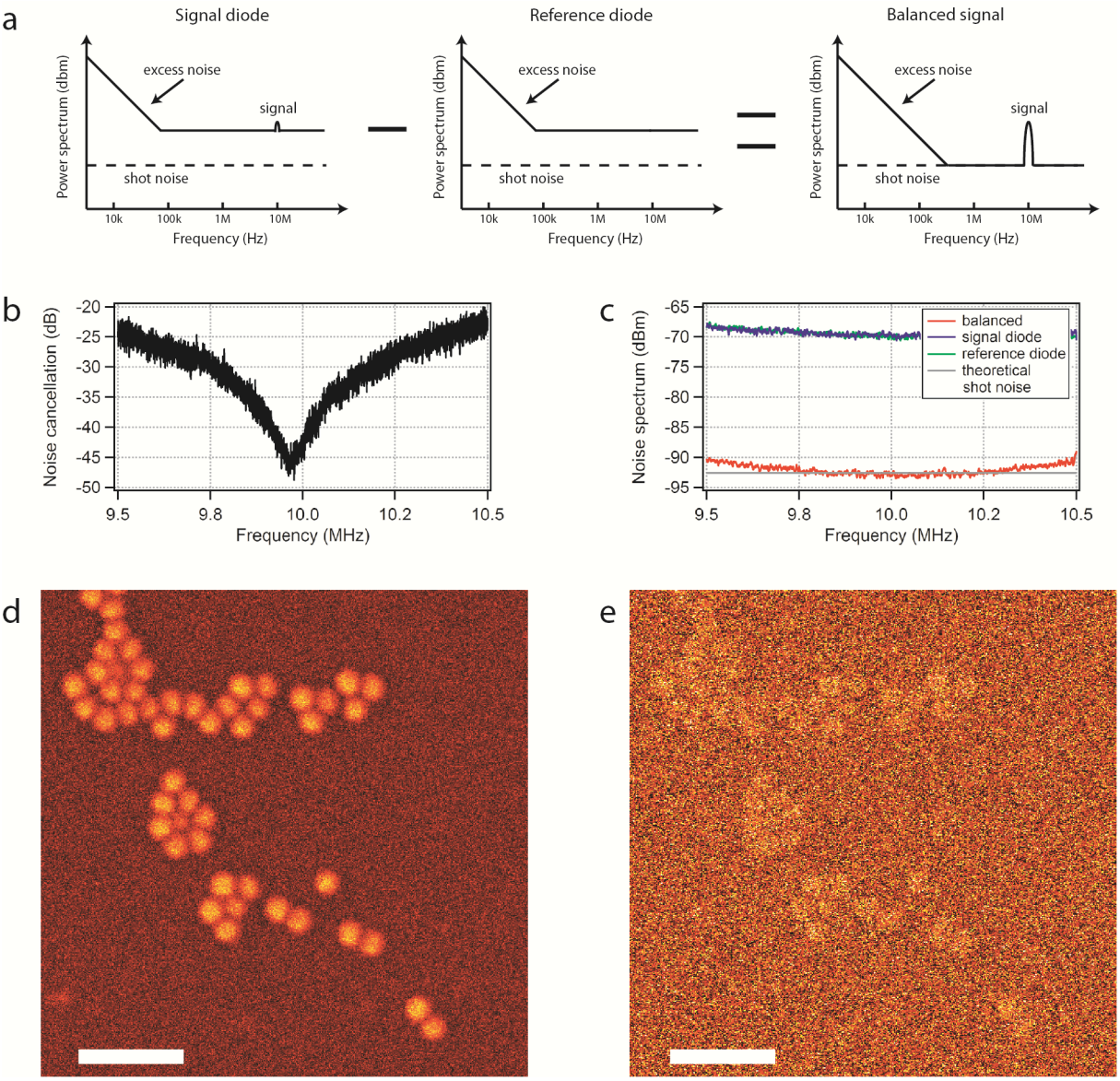


**Figure 3 | Auto-balanced detection. a**, Principle of balanced detection. **b** Noise suppression of the home-built auto-balanced detector optimized for 10MHz signal. **c** Noise spectrum of the fiber laser with (red) and without auto-balanced detection (blue). The theoretical shot-noise is indicated in grey. **d** & **e**, SRS image of 1.1μm polystyrene beads with (d) and without (e) auto-balanced detection. Scale bar: 5μm.

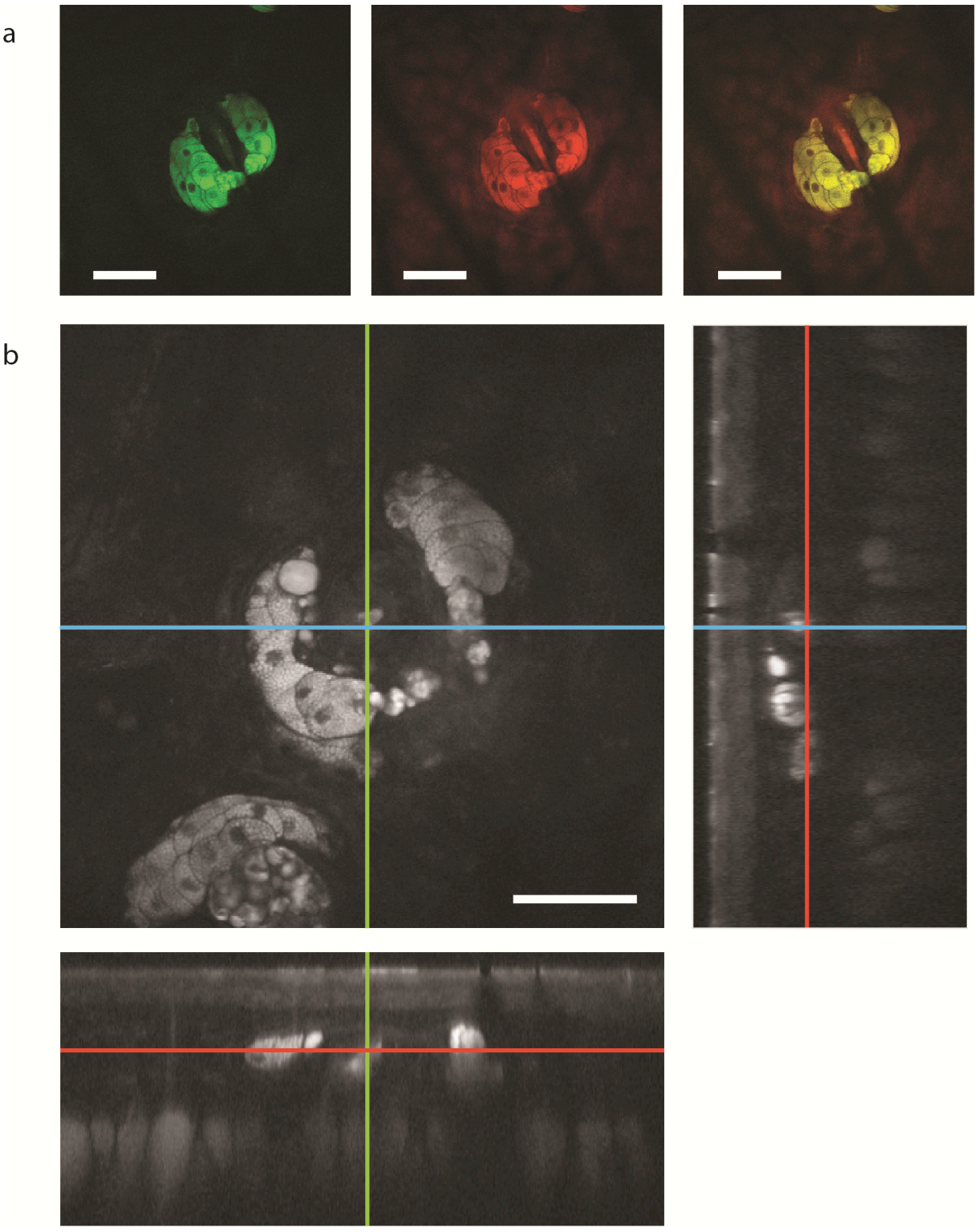


**Figure 4 | SRS spectral imaging with the fiber laser source. a**, Two color image of a sebaceous gland in mouse skin acquired at 2850cm$^{-1}$ (mainly lipids, green), 2950cm$^{-1}$ (mainly proteins, red) and

the composite of the two colors. **b**, z-stack acquired at 1 frame/s. Scale bar: 50μm, and cross-sections of different directions.